The W51 Giant Molecular Cloud

John M. Carpenter¹ email: carp@ifa.hawaii.edu

and

D. B. Sanders email: sanders@ifa.hawaii.edu Institute for Astronomy, 2680 Woodlawn Drive, University of Hawaii, Honolulu, HI 96822

ABSTRACT

We present 45"-47" angular resolution maps at 50" sampling of the ¹²CO and ^{13}CO J=1-0 emission toward a 1.39° \times 1.33° region in the W51 HII region complex. These data permit the spatial and kinematic separation of several spectral features observed along the line of sight to W51, and establish the presence of a massive $(1.2 \times 10^6 M_{\odot})$, large $(\Delta \ell \times \Delta b = 83 \,\mathrm{pc} \times 114 \,\mathrm{pc})$ giant molecular cloud (GMC), defined as the W51 GMC, centered at $(\ell, b, V)_c \sim (49.5^{\circ}, -0.2^{\circ}, 61 \text{ km s}^{-1})$. A second massive $(1.9 \times 10^5 M_{\odot})$, elongated (136 pc \times 22 pc) molecular cloud is found at velocities of \sim 68 km s⁻¹ along the southern edge of the W51 GMC. Of the five radio continuum sources that classically define the W51 region, the brightest source at $\lambda 6 \,\mathrm{cm}$ (G49.5-0.4) is spatially and kinematically coincident with the W51 GMC and three (G48.9-0.3, G49.1-0.4, and G49.2-0.4) are associated with the $68 \,\mathrm{km} \,\mathrm{s}^{-1}$ cloud. Published absorption line spectra indicate that the fifth prominent continuum source (G49.4-0.3) is located behind the W51 molecular cloud. The W51 GMC is among the upper 1% of clouds in the Galactic disk by size and the upper 5-10% by mass. While the W51 GMC is larger and more massive than any nearby molecular cloud, the average H₂ column density is not unusual given its size and the mean H₂ volume density is comparable to that in nearby clouds. The W51 GMC is also similar to other clouds in that most of the molecular mass is contained in a diffuse envelope that is not currently forming massive stars. We speculate that much of the massive star formation activity in this region has resulted from a collision between the 68 km s⁻¹ cloud and the W51 GMC.

¹Current Address: California Institute of Technology, Department of Astronomy, MS 105-24, Pasadena, CA 91125; jmc@astro.caltech.edu

Subject headings: ISM: clouds — ISM: general — ISM: individual (W51) —

ISM: molecules

1. Introduction

The compact radio continuum sources comprising W51 (Westerhout 1958) have long been recognized to constitute some of the most luminous star formation regions in the disk of the Galaxy (Harper & Low 1971; Hoffman, Frederick, & Emery 1971). The high luminosity, the large number of inferred O type stars (Bieging 1975), and the location of these sources within a molecular cloud (Mufson & Liszt 1979) all suggest that the W51 region represents the early formation stages of an OB association. Besides the intrinsic interest in the properties of W51, this region represents one of the closest analogs in the disk of the Milky Way to the more vigorous star forming sites found in other galaxies (e.g. 30 Doradus). Since these latter regions are quite distant, W51 affords many advantages in investigating the detailed properties of luminous star forming sites and inferring how these regions may originate.

One key to understanding the formation and evolution of any star forming region is establishing the properties of the molecular cloud out of which the stars form. While the molecular gas in the W51 region has been the subject of numerous studies, the interpretation of the results remain controversial. Scoville & Solomon (1973), primarily on the basis of small strip maps in $^{12}\text{CO}(1-0)$, identified several molecular line components toward W51 and derived a minimum mass of $10^5~\text{M}_\odot$ and a diameter $\sim 20-30~\text{pc}$ for the molecular cloud that they associated with the most intense radio component at $\lambda 6~\text{cm}$ (G49.5-0.4; Mehringer 1994). They further suggested that this cloud might be physically related to the several thermal radio continuum sources that make up the W51 H II-region complex (Goss & Shaver 1970; Wilson et al. 1970; Georgelin & Georgelin 1976). Subsequent studies of the molecular gas toward W51 have confirmed the existence of a large molecular cloud (Mufson & Liszt 1979; Nakamura et al. 1984; Ohishi et al. 1984; Dame et al. 1987; Solomon et al. 1987; Scoville et al. 1987), although various models continue to be proposed for the relationship of the multiple spectral features seen in the molecular gas lines and their association with the different H II regions.

The primary difficulty in establishing a definitive model of this region is the unique location of W51 in the Galaxy with respect to the sun. The W51 region has classically been associated with the tangent point of the Sagittarius spiral arm, which is oriented such

that the line of sight toward W51 intersects the spiral arm over several kiloparsecs of path length (Shane & Bieger-Smith 1966; Burton 1970). Much of the uncertainty surrounding the W51 region stems from establishing whether the numerous radio continuum sources and molecular clouds represent a single, large massive star forming region, or the chance projection of unrelated star forming sites viewed down a spiral arm. To better place the W51 region in context with respect to its location in the Galactic plane, Figure 1 displays the integrated ¹²CO(1–0) emission in 10 km s⁻¹ velocity bins covering longitudes 40°-55° from the Massachusetts-Stony Brook ¹²CO Survey (Sanders et al. 1986). The W51 region is distinguished by bright ¹²CO emission extending over a 1°×1° area centered on $(\ell, b) \sim (49.5^{\circ}, -0.2^{\circ})$ at velocities $\gtrsim 55 \,\mathrm{km \, s^{-1}}$. A "3-D" view of the (ℓ, b, V) ¹²CO data cube covering the region surrounding W51 is shown in Figure 2. The ¹²CO isointensity contour surface in this figure clearly illustrates both the relatively large number of smaller molecular clouds with typical internal velocity dispersions of $\Delta V \sim 3-5 \text{ km s}^{-1}$, and the large concentration of 12 CO emission extending over a $\sim 20\,\mathrm{km\,s^{-1}}$ interval in the W51 region. Much of the ¹²CO emission in this area has centroid velocities that exceed the maximum velocity permitted by pure circular rotation (i.e. $V_{\rm max} \sim 54-57 \,\rm km \, s^{-1}$; Brand & Blitz 1993). Such velocities have long been noted in 21 cm HI surveys at longitudes near $\ell = 50^{\circ}$, and have been attributed to large-scale streaming motions of gas in a spiral density wave (e.g. Shane & Bieger-Smith 1966; Burton 1970).

In principle the extent and properties of the molecular clouds located in the W51 region can be established by using the kinematic information in the molecular line data to isolate individual clouds. In practice, previous surveys have had either poor resolution or sparse sampling to make such an attempt feasible. Therefore, we have obtained full beam sampled maps of the W51 region in both $^{12}CO(1-0)$ and $^{13}CO(1-0)$ at subarcminute resolution in order to determine the relationship between the various molecular components. These maps permit us to disentangle the blends of unrelated clouds along the line of sight and to obtain more accurate mass estimates of the molecular gas. These data can also be compared with similar maps of more nearby clouds that have recently been obtained by us and others.

The outline of this paper is as follows. In Section 2, the observing procedures are described and channels maps of the ¹²CO and ¹³CO emission are presented. Analysis of the different spectral features observed in these maps and a more thorough discussion of the main features associated with the compact radio continuum sources in W51 is given in Section 3. In Section 4, we discuss the current massive star formation events in the region with respect to the various molecular components and comment on the evolution of the W51 Giant Molecular Cloud (GMC). Our conclusions are summarized in Section 5.

2. Observations

2.1. Observing Procedure

A 1.39° x 1.33° region (100 x 96 pixels) toward the W51 region was mapped in $^{12}\mathrm{CO}(1\text{--}0)$ (115.271203 GHz) and $^{13}\mathrm{CO}(1\text{--}0)$ (110.201370 GHz) in April 1995 using the QUARRY receiver array (Erickson et al. 1992) on the FCRAO 14 m telescope. The full width at half maximum beam size of the 14 meter antenna at these frequencies is 45″ and 47″ at 110 and 115 GHz respectively. The data were taken in position switching mode and calibrated with the standard chopper wheel method of observing an ambient temperature load and sky emission. The backends for each pixel of the array consisted of an autocorrelator spectrometer set to span the velocity range from $\sim 0\text{--}100\,\mathrm{km\,s^{-1}}$ at 78 kHz sampling (0.20 km s $^{-1}$ @ 115 GHz) and 94 kHz resolution (0.24 km s $^{-1}$). During data reduction the spectra were smoothed to a velocity resolution of 0.5 km s $^{-1}$.

Previous FCRAO measurements indicate that the spillover and scatter efficiency ($\eta_{\rm fss}$) of the telescope and radome is ~ 0.7 at the observed frequencies. The observed antenna temperatures corrected by $\eta_{\rm fss}$ are presented as $T_{\rm R}^*$ (Kutner & Ulich 1981). A further correction, the source coupling efficiency ($\eta_{\rm c}$), accounts for the coupling of the beam to the source. For a uniform source that fills only the main beam of the 14 m telescope, $\eta_{\rm c}$ is ~ 0.7 (i.e. 30% of the power is scattered on angular sizes much greater than the FWHM beam size), while for sources with uniform intensity over a diameter of 30', $\eta_{\rm c}$ is 1.0. In practice, the observed structures in the $^{12}{\rm CO}$ and $^{13}{\rm CO}$ maps span a range of sizes and shapes, and applying a single coupling efficiency for the entire map is incorrect. For simplicity, we present and analyze the data in the $T_{\rm R}^*$ temperature scale. The typical rms noise in the $^{12}{\rm CO}$ and $^{13}{\rm CO}$ maps in 0.5 km s⁻¹ channels is $\Delta T_{\rm R}^* \sim 0.7$ K and 0.6 K respectively.

2.2. The Data

Images of the integrated ^{12}CO and ^{13}CO intensity ($\int T_{\mathrm{R}}^* \ dv$) in $2\,\mathrm{km}\,\mathrm{s}^{-1}$ wide intervals are presented in Figures 3 and 4 respectively in the velocity range from 40 to $70\,\mathrm{km}\,\mathrm{s}^{-1}$. The values printed in the upper left corner of each figure panel denote the centroid velocity of the particular interval. Extended $^{12}\mathrm{CO}$ and $^{13}\mathrm{CO}$ emission was detected between $0\,\mathrm{km}\,\mathrm{s}^{-1}$ and $25\,\mathrm{km}\,\mathrm{s}^{-1}$, but these data are not presented here. This low velocity emission most likely originates from local molecular clouds and is not related to the W51 region of interest here. Little emission was observed between 25 and $35\,\mathrm{km}\,\mathrm{s}^{-1}$ and at velocities in excess of $75\,\mathrm{km}\,\mathrm{s}^{-1}$ (see §3). Similar velocity structure is also observed in the 21 cm H I emission

lines (Burton 1970). The following section analyzes the velocity structure in the molecular line maps and identifies individual molecular clouds.

3. Analysis

3.1. Velocity Structure

The ¹²CO and ¹³CO emission toward the W51 region contains a number of discrete velocity components that overlap in projection both spatially and kinematically. To identify and isolate the emission from these velocity components, multiple gaussians convolved with the spectrometer channel widths were fitted to each spectrum in an automated manner. The free parameters for each gaussian were the amplitude of the spectral line, the mean velocity, and the line width. The number of gaussians fitted to each spectrum was determined by searching for contiguous channels that contain an integrated intensity with a signal to noise ratio ≥ 3 . Channels containing a local antenna temperature maxima (denoted here as channels c_i , i = 1, n) in each such section were then identified. A local maximum at channel c_i was deemed a "significant" peak if the antenna temperature in any channel between c_i and the neighboring local maximum at channels c_{i-1} and c_{i+1} decreased by more than $2\sigma_{\rm rms}$ from the antenna temperature at channel c_i . The number of significant peaks corresponded to the number of gaussians fitted to that section. Each spectrum was smoothed to a velocity resolution of $1.5 \,\mathrm{km}\,\mathrm{s}^{-1}$ prior to identifying the peaks, although the fits were performed on the $0.5\,\mathrm{km\,s^{-1}}$ resolution data. Spectra with large residuals with respect to the gaussian fits were visually inspected and additional gaussians were added as appropriate. The ¹³CO data were easily decomposed into gaussians in this manner, but it often became difficult to reliably identify the velocity features in the heavily blended ¹²CO lines. Also, toward the compact H II regions, some of the structure in the ¹²CO and ¹³CO line profiles can be attributed to the absorption of radiation from hot molecular gas by colder foreground material (see Mufson & Liszt 1979). Away from these compact regions, absorption effects are not as significant, and over most of the cloud, the peaks in the spectral lines should accurately represent the velocity structure along the line of sight.

The results from the gaussian decomposition of the line profiles are synthesized in Figure 5. The upper panel shows histograms of the mean velocities for the 12 CO (thick lines) and 13 CO (thin lines) gaussians, and the lower panel shows the total integrated intensity in the gaussians as a function of the mean velocity. Most of the emission is confined to velocity intervals of $0-25\,\mathrm{km\,s^{-1}}$ and $35-75\,\mathrm{km\,s^{-1}}$. We identify the $0-25\,\mathrm{km\,s^{-1}}$ emission as originating from nearby molecular material and the $35-75\,\mathrm{km\,s^{-1}}$ emission with molecular gas in the Sagittarius spiral arm. Several velocity components occur repeatedly in both the

 12 CO and 13 CO gaussian fits as signified by the histogram peaks shown in the top panel in Figure 5. In particular, velocity components at 7, 15–25, 44, 49, 53, 60, 63, and 68 km s⁻¹ are readily apparent. In terms of the 12 CO and 13 CO integrated intensity, the two major features are the $60 \, \mathrm{km} \, \mathrm{s}^{-1}$ and $63 \, \mathrm{km} \, \mathrm{s}^{-1}$ components. A $58 \, \mathrm{km} \, \mathrm{s}^{-1}$ component is indicated as well since that is the centroid velocity of the molecular line emission toward the brightest radio continuum source in the W51 region (Mufson & Liszt 1979). Note, however, that the $58 \, \mathrm{km} \, \mathrm{s}^{-1}$ component is not a prominent feature as judged from Figure 5. The following discussion briefly highlights the morphology of the individual velocity components.

3.1.1. 7 and $15-25 \, km \, s^{-1}$ components

The $7 \,\mathrm{km}\,\mathrm{s}^{-1}$ velocity component contains weak, narrow lines over nearly the entire mapped region and is undoubtedly a nearby molecular cloud. The $15-25 \,\mathrm{km}\,\mathrm{s}^{-1}$ interval appears to contain a few distinct velocity features (see Fig. 5), but it is unclear whether or not these components are physically related.

$$3.1.2.$$
 $44 \, km \, s^{-1}$ component

The $44\,\mathrm{km\,s^{-1}}$ cloud is elongated parallel to the Galactic plane at $b=0^\circ$, although this cloud may form part of a larger structure that extends to lower Galactic latitudes. The molecular gas at these lower latitudes occurs at velocities of $\sim 40\,\mathrm{km\,s^{-1}}$, which is outside the velocity range assigned to this feature.

3.1.3.
$$49$$
 and $53 \,\mathrm{km} \,\mathrm{s}^{-1}$ components

The 12 CO emission from the 49 and $53\,\mathrm{km\,s^{-1}}$ components is more fragmented than the other features mentioned so far. These fragments may represent either individual clouds or the remnants of a once larger cloud in the Galactic plane. The $53\,\mathrm{km\,s^{-1}}$ cloud is distinguished by bright 12 CO emission near $(\ell,b)\sim(49.4^\circ,-0.3^\circ)$ that is associated with the compact H II region G49.4-0.3 (see §4.1).

3.1.4. 58, 60, and $63 \,\mathrm{km} \,\mathrm{s}^{-1}$ components: The W51 Giant Molecular Cloud

The $63\,\mathrm{km\,s^{-1}}$ component extends for nearly a degree in length and is found mainly in the central and eastern part of the mapped region. This is best observed in the $66\,\mathrm{km\,s^{-1}}$ panel shown in Figure 3, which represents the line wing emission of this velocity component (as well as emission from the $68\,\mathrm{km\,s^{-1}}$ cloud discussed below). The $60\,\mathrm{km\,s^{-1}}$ component consists predominantly of a diffuse patch of emission that extends into a filament to the east, and a second filament to the south. The $60\,\mathrm{km\,s^{-1}}$ and $63\,\mathrm{km\,s^{-1}}$ velocity components, along with the $68\,\mathrm{km\,s^{-1}}$ cloud discussed below, likely correspond to the "high velocity stream" of 21 cm H I emission (Burton 1970) that has been attributed to the streaming motions of gas down the Sagittarius spiral arm.

Careful inspection of the channel maps indicates that the spatial distribution of the $60\,\mathrm{km\,s^{-1}}$ and $63\,\mathrm{km\,s^{-1}}$ components generally do not overlap. For example, the western edge of the $63\,\mathrm{km\,s^{-1}}$ component closely matches the eastern edge of the $60\,\mathrm{km\,s^{-1}}$ emission. This is best seen in Figure 4 and the $60\,\mathrm{km\,s^{-1}}$ and $66\,\mathrm{km\,s^{-1}}$ velocity panels in Figure 3. Further, the extended emission from the eastern portion of the $63\,\mathrm{km\,s^{-1}}$ component is just above the filamentary extension of the $60\,\mathrm{km\,s^{-1}}$ component. Such interfaces are unlikely to occur by chance from two unrelated clouds along the line of sight, and suggest that the $60\,\mathrm{and}\,63\,\mathrm{km\,s^{-1}}$ components represent kinematic structure within a single molecular cloud. Velocity differences of this magnitude are commonly observed in nearby molecular clouds (e.g. Bally et al. 1987).

The $58 \,\mathrm{km} \,\mathrm{s}^{-1}$ component is dominated by bright, compact molecular emission and does not contain the diffuse extended emission that characterizes the 60 and $63 \,\mathrm{km}\,\mathrm{s}^{-1}$ features. Inspection of the channel maps suggests that this velocity component also reflects the interval kinematic structure within a single cloud encompassing the $60\,\mathrm{km}\,\mathrm{s}^{-1}$ and $63 \,\mathrm{km} \,\mathrm{s}^{-1}$ clouds. For example, the emission from the filament protruding to the southern portion of the mapped region contains primarily a centroid velocity of $58 \,\mathrm{km}\,\mathrm{s}^{-1}$ closest to bright compact ¹²CO and ¹³CO emission. Further away from this bright, compact emission region, the velocity of the filament changes to $\sim 60 \, \mathrm{km \, s^{-1}}$. Similar velocity patterns are observed in emission features along the eastern and western edges of the map. These results suggest that the emission constituting the 58, 60, and $63 \,\mathrm{km} \,\mathrm{s}^{-1}$ components represent the internal velocity structure within a single molecular cloud. Koo (1997) reached similar conclusions concerning the atomic hydrogen clouds at these velocities based upon HI absorption observations toward the radio continuum sources. Since the bright ¹²CO emission associated with the $58 \,\mathrm{km}\,\mathrm{s}^{-1}$ and $60 \,\mathrm{km}\,\mathrm{s}^{-1}$ components are coincident with the brightest radio continuum source in the W51 region (G49.5-0.5; see §4.1), we henceforth refer to the $58-60-63 \,\mathrm{km} \,\mathrm{s}^{-1}$ components as the W51 molecular cloud.

3.1.5. $68 \, \mathrm{km \, s^{-1}}$ component

The $68\,\mathrm{km\,s^{-1}}$ component extends for $\sim 1^\circ$ east—west across the image and also likely constitutes part of the "high velocity stream" identified in HI surveys (Burton 1970). Interestingly, the $68\,\mathrm{km\,s^{-1}}$ filament is located at the southern edge of the diffuse emission associated with the W51 molecular cloud at velocities $\gtrsim 63\,\mathrm{km\,s^{-1}}$ (see Figs. 3 and 4). Again, such a clear truncation of the W51 molecular cloud at the location of the $68\,\mathrm{km\,s^{-1}}$ cloud is unlikely to occur from two random clouds along the line of sight, and strongly suggests that these two clouds are physically related objects at a common distance. Nonetheless, the elongated appearance of the $68\,\mathrm{km\,s^{-1}}$ cloud is in stark contrast to the roughly circular shape of the W51 cloud, indicating that these two objects are best treated as individual structures rather than a single molecular cloud.

3.2. Properties of the W51 and the $68 \,\mathrm{km}\,\mathrm{s}^{-1}$ Molecular Clouds

The physical properties of the molecular clouds in the W51 region can be determined from the gaussian decomposition of the line profiles. We single out these two clouds since they contain four of the five bright HII regions found in radio continuum surveys (see $\S4.1$). In deriving the properties, the distance to the W51 cloud is assumed to be 7.0 ± 1.5 kpc as determined from proper motion studies of the W51 MAIN H₂O maser in the G49.5-0.4 dense core (Genzel et al. 1981). The $68\,\mathrm{km\,s^{-1}}$ cloud was assumed to have the same distance based on its apparent association with the W51 cloud as discussed above. The other clouds are not included in this analysis since their distances are unknown.

The properties of the W51 and $68\,\mathrm{km\,s^{-1}}$ clouds are summarized in Table 1. The cloud size represents a visual estimate of the extent of the detectable $^{12}\mathrm{CO}$ emission along the major (θ_{max}) and minor (θ_{min}) axis of the cloud. The cloud line width, ΔV_{FWHM} , is the full width at half maximum of the sum of the gaussian fits comprising the respective clouds. Two estimates of the cloud mass are provided in Table 1. The virial mass, M_{vir} , was calculated using the expression $M_{\mathrm{vir}}=209\,R\,\Delta V^2\,M_{\odot}$, where ΔV is the full width at half maximum line width in kilometers per second and R is the cloud radius ($\equiv\sqrt{\theta_{\mathrm{max}}\theta_{\mathrm{min}}}/2.0$) in parsecs at the zero intensity level. While the cloud size is actually measured at a finite $^{12}\mathrm{CO}$ intensity level, we find it unlikely that the clouds are appreciably larger at lower intensities, and no correction to the observed cloud size was applied. Note that the above expression for the virial mass is appropriate for a uniform density, spherical cloud. The equivalent expression for a r^{-1} and r^{-2} density cloud would decrease the constant factor in the virial mass expression to 188 and 125 respectively.

A second mass estimate can in principal be obtained from the ¹²CO and ¹³CO data using the LTE analysis (Dickman 1978). However, in blended regions, it is often difficult to associate 12 CO gaussian fits with analogous 13 CO features. Therefore, the H_2 column densities were estimated by applying a constant conversion factor to the ¹²CO integrated intensities (Dickman 1975; Solomon et al. 1987; Strong et al. 1988). To ensure that the Galactic conversion factor is indeed valid for the W51 region, the conversion factor was estimated from lines of sight with unblended ¹²CO and ¹³CO lines in the 56–71 km s⁻¹ velocity interval that defines the W51 and $68 \, \mathrm{km \, s^{-1}}$ clouds. The $\mathrm{H_2}$ column densities for these lines of sight were estimated using the procedure outlined by Dickman (1978) and assuming a 13 CO/H₂ abundance of 1.5 x 10^{-6} . A histogram of the ratio of the H₂ column densities to ¹²CO integrated intensities is strongly peaked with a mean value of $1.7 \times 10^{20} \text{ cm}^{-2} \text{ (K km s}^{-1})^{-1}$, and is similar to the conversion factor that has been derived for the Galaxy (between $\sim 2\text{--}3 \times 10^{20} \text{ cm}^{-2} \text{ (K km s}^{-1})^{-1}$; Strong et al. 1988 and references therein). The masses $(M_{\rm XCO})$ computed from the $^{12}{\rm CO}$ integrated intensities were calculated by adopting the conversion factor derived from the W51 data, and include a multiplicative factor of 1.36 to incorporate the mass contribution from heavier elements.

The results summarized in Table 1 indicate that the W51 molecular cloud has a mean diameter of ~ 97 pc and a mass² of $\sim 10^6~M_{\odot}$. The similarity in the two mass estimates indicate the gravitational potential energy is approximately equal to the kinetic energy, and that self–gravity must play a critical role in the evolution of the W51 molecular cloud. The $68~\rm km~s^{-1}$ cloud is 136 pc in length but only 22 pc wide over most of the minor axis. Such an obvious departure from spherical symmetry renders the virial mass estimate suspect, and so the mass of the $68~\rm km~s^{-1}$ cloud was estimated only using the $^{12}\rm CO$ conversion factor. The mass obtained, $\sim 10^5~M_{\odot}$, is an order of magnitude less than that of the W51 cloud.

A comparison of the W51 cloud properties with the size and mass spectrum of molecular clouds in the Galaxy (e.g. Sanders, Scoville, & Solomon 1985; Solomon et al. 1987) shows that the W51 molecular cloud is one the largest GMCs in the Galactic disk. Among the ~ 5000 molecular clouds with diameters in excess of ~ 22 pc (and corresponding masses $\sim 10^5~M_{\odot}$; i.e. GMCs), the W51 GMC is in the upper 1% of the clouds by size and the upper 5–10% by mass. For the 68 km s⁻¹ cloud, although its mass is typical of a relatively low mass GMC, a distinguishing feature is its shape. The ratio of the major to minor axis of the 68 km s⁻¹ cloud is ~ 6 . In the cloud catalog by Solomon et al. (1987), 85% of the

 $^{^2}$ The virial mass derived here agrees well with that estimated by Dame et al. (1987), but is a factor of 4 less than found by Solomon et al. (1987). Solomon et al. (1987) derived a substantially larger velocity dispersion, and hence computed a larger virial mass, most likely by including the emission from the $68 \,\mathrm{km}\,\mathrm{s}^{-1}$ cloud and several other velocity components that we did not associate with the W51 molecular cloud.

clouds have an aspect ratio less than 2, and only one object has an aspect ratio greater than observed for the $68\,\mathrm{km\,s^{-1}}$ cloud. Clearly an elongated shape over such a large length scale is unusual in the molecular interstellar material and may indicate that the $68\,\mathrm{km\,s^{-1}}$ cloud is a transient structure originating from a relatively recent dynamical event.

4. Discussion

4.1. Massive Star Formation in the W51 Region

Now that the individual molecular clouds in the W51 region have been identified, their relationship to the massive star forming sites can be explored. Three images of the W51 region are shown in Figure 6: a map of the integrated ¹²CO(1–0) intensity generated from gaussian fits with mean velocities between 56 and $71 \,\mathrm{km}\,\mathrm{s}^{-1}$ (i.e. the W51 and $68 \,\mathrm{km} \,\mathrm{s}^{-1}$ clouds), an image of the $60 \,\mu\mathrm{m}$ emission from the IRAS Sky Survey Atlas, and a $\lambda 21$ cm radio continuum image (Koo & Moon 1997). The bulk of the 60μ m emission is elongated parallel to, but slightly below, the galactic plane, and is coincident with bright radio continuum emission. Of the sources labeled in the $\lambda 21$ cm continuum map, W51C has predominantly a non-thermal continuum spectrum and is thought to be a supernova remnant (Subrahmanyan & Goos 1995), while the other sources have thermal spectra and are compact HII regions. The radio continuum sources G49.4-0.3 and G49.5-0.4 are classically referred to as W51A (Kundu & Velusamy 1967), with the G49.5-0.4 region containing the infrared source W51 IRS1 (Wynn-Williams, Becklin, & Neugebauer 1974) and the H₂O masers W51 North, W51 South, and W51 MAIN (Genzel & Downes 1977). Sources G48.9-0.3, G49.1-0.4, and G49.2-0.4 are collectively known as W51B (Kundu & Velusamy 1967). The observed radio continuum fluxes (Koo 1997) and far-infrared luminosities ($\sim 10^{6-7} L_{\odot}$; Rengarajan et al. 1984; Harvey et al. 1986) imply the presence of one or more O stars in each of these regions.

Figure 6 shows that many of the radio continuum sources have corresponding peaks in the molecular line and far–infrared images. In addition to the spatial coincidences, these radio continuum sources have recombination line velocities (Wilson et al. 1970) similar to the velocity components identified from the ¹²CO observations. The G49.5-0.4 H II region has a recombination line velocity of 59 km s⁻¹ and is spatially coincident with the strong ¹²CO emission associated with the W51 molecular cloud. The recombination line velocities toward G48.9-0.3, G49.1-0.4, and G49.2-0.4 are 66, 72, and 66 km s⁻¹ respectively and are located along the 68 km s⁻¹ molecular cloud. Finally, the G49.4-0.3 H II region has a recombination line velocity of 53 km s⁻¹ and is coincident with the bright ¹²CO and ¹³CO emission from the 53 km s⁻¹ molecular cloud. (Note that the molecular gas associated with

this H II region is outside the velocity range that defines the W51 GMC.) H I (Koo 1997 and H_2CO (Arnal & Goss 1985) spectra toward this source exhibit absorption features at velocities of 63-65 km s⁻¹, indicating that G49.4-0.3 must be located behind the W51 GMC. However, these observations do not indicate whether this source is situated just beyond W51 and hence is physically related to the H II region complex, or if it is a distant, unrelated background massive star forming site. The molecular line maps presented here provide no compelling reason for (or against) such an association.

To search for any additional massive star forming sites in the W51 molecular cloud, the IRAS Point Source catalog was examined for objects that have at least two "high" quality detections among the four IRAS bands and a rising spectral energy distribution toward longer wavelengths. These criteria were designed to select a reliable sample of objects with far-infrared colors characteristic of embedded star forming regions (Walker et al. 1989). Of the 40 IRAS point sources within the mapped region that meet these criteria, the seven brightest objects at $25\mu m$ are located along the interface between the W51 and the $68 \,\mathrm{km \, s^{-1}}$ clouds. Visual inspection of IRAS $60\mu m$ image in Figure 6 confirms that the brightest sources are located along this ridge. Assuming that the other point sources are located at the distance of the W51 molecular cloud (although many of them are almost certainly foreground objects), point sources found away from this interface have far-infrared luminosities in the four IRAS bands less than $40,000 \, L_{\odot}$ and inferred spectral types later than ZAMS B0.5 (Vacca, Garmany, & Shull 1996). Thus embedded O type stars in the W51 region currently are confined to the southern extreme of the molecular cloud.

4.2. Comparison to Other Molecular Clouds

The extreme star formation characteristics of the W51 region raises the question as to whether the star formation activity stems from unusual global properties in the W51 molecular cloud, or from unusual conditions found local to the massive star forming sites. These possibilities can be explored by comparing the W51 cloud properties with other star forming regions that have also been extensively mapped in ¹²CO and ¹³CO. In particular, we shall compare the W51 and 68 km s⁻¹ clouds with the molecular clouds associated with the H II regions Sh 140, Sh 155, Sh 235, Sh 247, Sh 252, and Sh 255 which have been mapped with the same receiver and telescope used for the W51 observations (Heyer, Carpenter, & Ladd 1996; Carpenter, Snell, & Schloerb 1995). The embedded high mass stellar content in this comparison sample is generally limited to a single early–B/late O–type star and is in stark contrast to the cluster of O stars forming in the W51 molecular cloud.

The clouds in the comparison sample have diameters of ~ 20 –55 pc and masses of $\sim 2\times 10^4$ to 7×10^4 M_{\odot} . Thus the W51 molecular cloud is $\gtrsim 2.5$ times larger and $\gtrsim 10$ times more massive than these objects. Note that the molecular clouds associated with Sh 247, Sh 252, and Sh 255 are distinct regions within the Gem OB1 cloud complex, which has a total mass of 3×10^5 M_{\odot} and a diameter of ~ 150 pc (Carpenter, Snell, & Schloerb 1995). While the spatial size of the Gem OB1 complex is larger than the W51 cloud, the W51 cloud exhibits a continuous structure ~ 100 pc in size as opposed to the fragmentary appearance of the Gem OB1 complex. The $68\,\mathrm{km\,s^{-1}}$ cloud is also more massive than the objects in the comparison sample and is significantly more elongated than any of the clouds considered here. Thus the W51 and $68\,\mathrm{km\,s^{-1}}$ clouds are at the extreme in terms of cloud masses and sizes compared to objects in this sample. With the possible exception of the $68\,\mathrm{km\,s^{-1}}$ cloud, these clouds are similar though in that they appear to be gravitationally bound.

The size and mass of a cloud are not necessarily the key parameters that control the star formation activity within the cloud. Intuitively, one might expect that the amount of matter above a critical density to be the critical variable for otherwise similar clouds. Thus if the massive star formation activity in W51 has resulted from the large scale collapse of the cloud, one would expect the volume and column density densities to be larger than found in a typical cloud. As an indirect measure of the H₂ column densities, Figure 7 shows histograms of the observed 13 CO integrated intensities for each of the clouds in our sample. The lowest integrated intensity shown for any cloud is $3~{\rm K\,km\,s^{-1}}$ since that is approximately the highest 3σ detection limit among the various ¹³CO surveys. Comparison of the ¹²CO and ¹³CO intensities suggests that the ¹³CO emission is optically thin if the 12 CO and 13 CO excitation temperatures are equal as assumed in the LTE analysis (see Dickman 1978). Therefore, the distribution of ¹³CO integrated intensities should accurately trace the H₂ column density distributions as along as the ¹³CO abundance is roughly constant within a cloud. The ¹³CO integrated intensities in Figure 7 can be converted to $\rm H_2$ column densities for an assumed $^{13}{\rm CO/H_2}$ abundance of 1.5 x 10^{-6} (Bachiller & Cernicharo 1986) with the formula

$$N({\rm H_2}) = 3.05 \times 10^{19} T_{\rm ex} e^{5.29/T_{\rm ex}} \int T_{\rm R}^* (^{13}{\rm CO}) dv \ {\rm cm^{-2}}.$$

For an excitation temperature of $T_{\rm ex}=10$ K, the 3 K km s⁻¹ integrated intensity limit imposed for Figure 7 corresponds to an H₂ column density of 1.5 x 10^{21} cm⁻², or an visual extinction of $\sim 1.5^{\rm m}$ (Bohlin, Savage, & Drake 1978). Variations in the ¹³CO abundance and excitation conditions will obviously effect the absolute conversion from ¹³CO integrated intensities to H₂ column densities, and the comparisons here are intended to search for large differences (factors of several or more) in the typical column densities in these clouds.

Figure 7 shows that the distributions of 13 CO integrated intensities peak near the detection limit of 3 K km s⁻¹ for each cloud, with a long tail toward the higher integrated intensities. The tail of these distributions correspond to the high column density regions and are often associated with star forming sites. The mean 13 CO integrated intensity among the clouds varies between 4.9 and 9.7 K km s⁻¹, with the W51 cloud containing the third highest mean intensity and the $68 \, \mathrm{km \ s^{-1}}$ cloud the highest. The high values found for the $68 \, \mathrm{km \ s^{-1}}$ cloud may be a result of an unusual viewing angle, as either this cloud is a sheet of gas observed edge on or a long, narrow filament. These results imply that most of the mass in each cloud is contained in lines of sight with column densities corresponding to less than a few magnitudes of visual extinction. Thus the W51 GMC is similar to other clouds in that the diffuse envelope contains more mass than the high column density cores.

While the W51 cloud contains a higher column density on average than the other clouds, this can attributed to the fact that it is more than twice as large as some clouds in the sample. Indeed, assuming that the $1.2 \times 10^6~M_{\odot}$ W51 cloud is distributed in a sphere of diameter of 97 pc (see Table 1), the average $\rm H_2$ volume density is 40 cm⁻³, comparable to the volume density inferred in nearby molecular clouds (Blitz 1991; Carpenter, Snell, & Schloerb 1995). This suggests that the entire W51 molecular is probably not in an advanced stage of collapse, and that the intense star formation activity in W51 likely results from forces acting on a localized region. In retrospect, this is perhaps not surprising given that the massive star forming regions in W51 are located at the edge of the cloud and not in the center as expected if, for example, the entire cloud was systematically collapsing.

Contrary to the global properties, the gas properties local to the W51 massive star forming regions do appear to be unusual compared to the molecular clouds in the solar neighborhood. Submillimeter continuum observations have shown that the core containing the G49.5-0.4 H II region contains $\sim 10^5~M_{\odot}$ of gas with a mean H₂ volume density of $\sim 5~\rm x~10^4~cm^{-3}$ over a 3 pc radius region (Sievers et al. 1991). By contrast, submillimeter observations indicate that the most massive cores in nearby molecular clouds typically have masses $\sim 2-3$ orders of magnitude less than that of the G49.5-0.4 core (e.g. Oldham et al. 1994; Mezger et al. 1992; Schloerb, Snell, & Schwartz 1987; Jaffe et al. 1984). While the G49.5-0.4 core does not necessarily contain higher gas densities, it does contain more gas at the densities needed to form stars.

4.3. Evolution of the W51 Molecular Cloud

The above discussion suggests that the key to understanding the massive star formation activity in the W51 complex is determining the forces that acted on a localized region

within the cloud. The molecular line maps presented here allow us to speculate on what these forces may be. As shown in Figures 3 and 4, the diffuse emission from the W51 GMC truncates at the location of the $68 \,\mathrm{km} \,\mathrm{s}^{-1}$ cloud for velocities $\gtrsim 63 \,\mathrm{km} \,\mathrm{s}^{-1}$. This morphology was used in §3 to argue that the W51 and $68 \,\mathrm{km} \,\mathrm{s}^{-1}$ clouds are at a common distance since such an interface is unlikely to result from the chance superposition of unrelated molecular clouds. One way such an interface could form is if the $68 \,\mathrm{km} \,\mathrm{s}^{-1}$ cloud has collided into the W51 GMC (see also Arnal & Goss 1985; Pankonin, Payne, & Terzian 1979). Molecular gas does extend below the $68 \,\mathrm{km} \,\mathrm{s}^{-1}$ cloud at lower velocities, however. In this picture, given the three dimensional structure of the W51 GMC, this material has not crossed the path of the $68 \,\mathrm{km} \,\mathrm{s}^{-1}$ cloud. Both H₂CO and HI spectra toward the G49.5-0.4 HII region (Koo 1997; Arnal & Goss 1985; Mufson & Liszt 1979) contain absorption lines at velocities $\gtrsim 65 \,\mathrm{km} \,\mathrm{s}^{-1}$, and relative to the line of sight, the $68 \,\mathrm{km} \,\mathrm{s}^{-1}$ cloud must be located in front of the W51 GMC. Since the velocity difference between the two clouds (at least 5 km s⁻¹) is larger than the sound speed, a shock front will form that will compress the molecular gas and possibly induce star formation (Elmegreen & Elmegreen 1978).

The qualitative model of two colliding clouds accounts for several properties of the W51 region. First, one would expect that star formation should occur preferentially along the interface region. The IRAS image in Figure 6 shows that this is indeed the case for massive stars, as the northern half of the W51 GMC appears devoid of embedded O type stars despite containing most of the cloud mass. The cloud collision model would also suggest that the massive star forming regions along the collision interface should have a common age. While the ages of these stars are not known, the lifetime of the mid-O type stars found in the W51 region (Mehringer 1994; see also Koo 1997) places an upper limit to the stellar ages of ~ 5 Myr (Meynet et al. 1994). The actual ages may be considerably less since these O stars are still in the compact HII region phase, which has a lifetime of less than 1 Myr (Churchwell 1990; Comerón & Torra 1996). Further support for a cloud-cloud collision model comes from considering the projected distance (73 pc) between the two furthest separated star forming regions along the $W51/68 \,\mathrm{km}\,\mathrm{s}^{-1}$ cloud interface. The sound travel time across this distance is nearly two orders of magnitude larger than the O star lifetime. Therefore, these star forming regions must have been created by either a single event operating along the entire southern edge of the cloud or from up to 4 separate. but nearly simultaneous, events. Given the scarcity of embedded O stars in the Galaxy, the cloud-collision model would provide a natural explanation for simultaneous star formation along the ridge. Ultimately, the suggested collision between the W51 and $68\,\mathrm{km\,s^{-1}}$ clouds may be related to a spiral density wave. The anomalous gas velocities in the W51 region have long been attributed to streaming motions in the Sagittarius spiral arm (Shane & Bieger-Smith 1966; Burton 1970). The associated spiral density wave may have indirectly

led to the massive star formation activity in the W51 region by enhancing the number density of clouds and increasing the probability of a cloud-cloud collision. Further, a spiral wave shock, if present (see Lubow, Balbus, & Cowie 1986), will compress and flatten any clouds (Woodward 1977). Indeed, such a shock could account for the highly elongated shape of the 68 km s⁻¹ cloud. The W51 GMC, however, remains roughly circular in shape, and globally its evolution is likely still dominated by self gravity.

Finally, we briefly consider the implications of these results for other star forming regions. While the W51 star forming region exceeds all nearby embedded star forming sites in terms of the number of O stars, bolometric luminosity, and dense core mass, W51 itself is dwarfed by some star forming regions in nearby galaxies. Most notably, the 30 Doradus region in the Large Magellanic cloud contains an order magnitude more O stars than W51 (Vacca et al. 1995). At larger distances, many interacting galaxies contain even yet more vigorous massive star forming regions that may be dense enough to represent young globular clusters (Whitmore et al. 1993). Most of the molecular gas appears to have been dispersed in these clusters already, and in any event, the distances to these systems precludes any detailed studies of the natal clouds. The most significant piece of information afforded by the W51 molecular maps is that despite containing one of the most massive dense cores known in our Galaxy, most of the mass in the W51 molecular cloud is not currently forming massive stars. Thus it is easy to imagine that the increase in the number of cloud-cloud collisions that presumably results in interacting galaxies may lead to a larger number of star forming regions throughout a single cloud or more intense star formation activity within a small region. In fact, the mass within the W51 molecular cloud is comparable to that in globular clusters, and it may not require the conglomeration of many giant molecular clouds to form these stellar systems, but the large scale collapse of a single GMC.

5. Summary

We have mapped a 1.39° x 1.33° region toward the W51 H II region complex at 45''-47'' resolution and 50'' sampling in the J=1–0 transitions of 12 CO and 13 CO. From these data we have identified the major molecular clouds and have associated these clouds with the massive embedded star forming sites in the W51 region. We find that:

(1) The two most prominent clouds in the W51 region are the $58\text{-}60\text{-}63\,\mathrm{km\,s^{-1}}$ cloud (defined as the W51 GMC) and the $68\,\mathrm{km\,s^{-1}}$ cloud. The W51 GMC is associated with the brightest $\lambda\,6\,\mathrm{cm}$ continuum source in W51 (G49.5-0.4), and the $68\,\mathrm{km\,s^{-1}}$ cloud contains the H II regions G48.9-0.3, G49.1-0.4, and G49.2-0.4. Published absorption line spectra (Koo 1997; Arnal & Goss 1985) indicate that the fifth bright H II region in the area,

G49.4-0.3, must be located behind the W51 GMC, but it remains unclear whether or not it is physically associated with the other star forming regions.

- (2) The mass of the W51 GMC and the $68\,\mathrm{km\,s^{-1}}$ clouds are $\sim 1.2\times 10^6~M_\odot$ and $1.9\times 10^5~M_\odot$ respectively. The W51 molecular cloud is roughly circular in shape with a mean diameter of ~ 97 pc and appears to be gravitationally bound. Compared to the ~ 5000 GMCs in the Galactic disk, W51 is among the top 1% by size and the top 5–10% in terms of cloud mass. The $68\,\mathrm{km\,s^{-1}}$ cloud is an elongated filament of $\sim 136\,\mathrm{pc}\times 22\,\mathrm{pc}$ in size. The 6:1 aspect ratio of the major and minor axis in the $68\,\mathrm{km\,s^{-1}}$ are rare in the Galaxy over such a large size scale (Solomon et al. 1987), and suggests that this molecular cloud may represent a transient feature.
- (3) The properties of the W51 and $68 \,\mathrm{km}\,\mathrm{s}^{-1}$ clouds are compared with nearby clouds that have been studied in a similar manner but contain lower levels of massive star formation activity. While the W51 cloud is larger and more massive than nearby clouds, the mean H_2 column density is not unusual given the large size, and the mean H_2 volume density is comparable. The W51 GMC is similar to other clouds in that most of the molecular mass is contained in a diffuse molecular envelop that is not forming massive stars. The $68 \,\mathrm{km}\,\mathrm{s}^{-1}$ cloud contains the largest mean column density among the clouds studied here, but this may be a result of an unusual viewing angle for this elongated cloud. We suggest that much of the star formation activity in the W51 region has not resulted from global collapse of the W51 cloud, but from forces acting on localized regions within the cloud.
- (4) We speculate that much of the massive star formation activity in W51 has resulted from a collision between the W51 and $68 \,\mathrm{km}\,\mathrm{s}^{-1}$ molecular clouds. This conjecture can explain the string of embedded O stars that are spread out for 70 pc along the interface between the W51–68 km s⁻¹ clouds, and why massive star formation is currently confined to the southern ridge of the W51 GMC.

We would like to thank Mark Heyer for completing the 13 CO map of W51 and Bon–Chul Koo for making available his $\lambda 21$ cm continuum image of W51. JMC acknowledges support from the James Clerk Maxwell Telescope Fellowship. DBS was supported in part by NASA grant NAGW-3938. The Five College Radio Astronomy Observatory is operated with support from NSF grant 94–20159.

REFERENCES

Bachiller, R. & Cernicharo, J. 1986, A&A, 166, 283

Bally, J., Stark, A. A., Wilson, R. W., & Langer, W. D. 1987, ApJ, 312, L45

Bieging, J. 1975, in Lecture Notes in Physics 42, HII Regions and Related Topics, ed. T. L. Wilson and D. Downes (Berlin: Springer), 443

Blitz, L. 1991, in The Physics of Star Formation, eds. C. J. Lada & N. Kylafis, (Dordrecht:Kluwer), 1

Bohlin, R. C., Savage, B. D., & Drake, J. F. 1978, ApJ, 224, 132

Brand, J., & Blitz, L. 1993, A&A, 275, 67

Burton, W. B. 1970, A&AS, 2, 291

Carpenter, J. M., Snell, R. L., & Schloerb, F. P. 1995, ApJ, 445, 246

Churchwell, E. 1990, A&A Rev., 2, 79

Comerón, F. & Torra, J. 1996, A&A, 314, 776

Dame, T. M., Ungerechts, H., Cohen, R. S., De Geus, E. J., Grenier, I. A., May, J., Murphy, D. C., Nyman, L.-Å, & Thaddeus, P. 1987, ApJ, 322, 706

Dickman, R. L. 1975, ApJ, 202, 50

Dickman, R. L. 1978, ApJS, 37, 407

Elmegreen, B. G., & Elmegreen, D. M. 1978, ApJ, 220, 1051

Erickson, N. R., Goldsmith, P. F., Novak, G., Grosslein, R. M., Viscuso, P. J., Erickson, R. B., & Predmore, C. R. 1992, IEEE Trans. on Microwave Theory and Techniques, 40, 1

Genzel, R., & Downes, D. 1977, A&AS, 30, 145

Genzel, R., Downes, D., Schneps, M. H., Reid, M. J., Moran, J. M., Kogan, L. R., Kostenko, V. I., Matveyenko, L. I., & Rönnäng, B. 1981, ApJ, 247, 1039

Georgelin, T. M., & Georgelin, Y. P. 1976, A&A, 49, 57

Goss, W. M., & Shaver, P. A. 1970, Australian J. Phys, Ap. Suppl., 14, 1

Harper, D. A., & Low, F. J. 1971, ApJ, 165, L9

Harvey, P. M., Joy, M., Lester, D. F., & Wilking, B. A. 1986, ApJ, 300, 737

Heyer, M. H., Carpenter, J. M., & Ladd, E. F. 1996, ApJ, 463, 630

Hoffman, W. F., Frederick, C. L., & Emery, R. J. 1971, ApJ, 170, L89

Jaffe, D. T., Davidson, J. A., Dragovan, M., & Hildebrand, R. H. 1984, ApJ, 284, 637

Koo, B. 1997, ApJS, 108, 489

Koo, B., & Moon, D. 1997, ApJ, 475, 194

Kundu, N. R., & Velusamy, T. 1967, Ann. d'Astrophys. 30, 59

Kutner, M. L., & Ulich, B. K. 1981, ApJ, 250, 341

Lubow, S. H., Balbus, S. A., & Cowie, L. L. 1986, ApJ, 309, 496

Mehringer, D. M. 1994, ApJS, 91, 713

Meynet, G., Maeder, A., Schaller, G., Schaerer, D., & Charbonnel, C. 1994, A&AS, 103, 97

Mezger, P. G., Sievers, A. W., Haslam, C. G. T., Kreysa, E., Lemke, R., Mauersberger, R., & Wilson, T. L. 1992, A&A, 256

Mufson, S. L., & Liszt, H. S. 1979, ApJ, 232, 451

Nakamura, T., Kodaira, S., Ishi, K., Inatani, J., & Ohishi, M. 1984, PASJ, 36, 123

Ohishi, M., Nakamura, T., Kodaira, S., Ishi, K., & Inatani, J. 1984, PASJ, 36, 505

Oldham, P. G., Griffin, M. J., Richardson, K. J., & Sandell, G. 1994, A&A, 284, 559

Pankonin, V., Payne, H. E., & Terzian, Y. 1979, A&A, 75, 365

Rengarajan, T. N., Cheung, L. H., Fazio, G. G., Shivanandan, K., McBreen, B. 1984, ApJ, 286, 573

Sanders, D. B., Clemens, D. P., Scoville, N. Z., & Solomon, P. M. 1986, ApJS, 60, 1

Sanders, D. B., Scoville, N. Z., & Solomon, P. M. 1985, ApJ, 289, 373

Schloerb, F. P., Snell, R. L., & Schwartz, P. R. 1987, ApJ, 319, 426

Scoville, N. Z. & Solomon, P. M. 1973, ApJ, 180, 31

Scoville, N. Z., Yun, M. S., Clemens, D. P., Sanders, D. B., & Waller, W. H. 1987, ApJS, 63, 821

Shane, W. W. & Bieger-Smith, G. P. 1966, Bull. Astron. Inst. Netherlands, 18, 263

Sievers, A. W., Mezger, P. G., Gordon, M. A., Kreysa, E., Haslam, C. G. T., & Lemke, R. 1991, A&A, 251, 231

Solomon, P. M., Rivolo, A. R., Barrett, J., & Yahil, A. 1987, ApJ, 319, 730

Strong, A. W., Bloemen, J. B. G. M., Dame, T. M., Grenier, I. A., Hermsen, W., Lebrun, F., Nyman, L.-Å., Pollock, A. M. T., & Thaddeus, P. 1988, A&A, 207, 1

Subrahmanyan, R. & Goss, W. M. 1995, MNRAS, 275, 755

Vacca, W. D., Robert, C., Leitherer, C., & Conti, P. S. 1995, ApJ, 444, 647

Vacca, W. D., Garmany, C. D., & Shull, J. M. 1996, ApJ, 460, 914

Walker, H. J., Cohen, M., Volk, K., Wainscoat, R. J., & Schwartz, D. E. 1989, AJ, 98, 2163

Westerhout, G. 1958, Bull. Astron. Inst. Netherlands, 14, 215

Whitmore, B. C., Schweizer, F., Leitherer, C., Borne, K., & Robert, C. 1993, AJ, 106, 1354

Wilson, T. L., Mezger, P. G., Gardner, F. F., & Milne, D. K. 1970, Astrophys. Lett., 5, 99

Woodward, P. R. 1976, ApJ, 207, 484

Wynn-Williams, C. G., Becklin, E. E., & Neugebauer, G. 1974, ApJ, 187, 473

This preprint was prepared with the AAS LATEX macros v4.0.

- Fig. 1.— Galactic longitude–latitude images of $^{12}\text{CO}(\text{J}=1-0)$ integrated intensity ($\int T_{\text{R}}^* dv$) in 10 km s⁻¹ intervals along the Galactic midplane ($|b| \leq 1^{\circ}$) from $\ell = 40^{\circ} 55^{\circ}$. The data are from the Massachusetts–Stony Brook Galactic Plane Survey (Sanders et al. 1986). The W51 GMC complex is seen most clearly in the $\Delta V = 55 65 \text{ km s}^{-1}$ panel as bright ^{12}CO emission that extends over $\sim 1^{\circ}$ x 1° centered near $\ell = 49.5^{\circ}$, $b = -0.2^{\circ}$. A high velocity "ridge" of ^{12}CO emission is evident in the $\Delta V = 65 75 \text{ km s}^{-1}$ panel at the same ℓ and b.
- Fig. 2.— A 3-dimensional, velocity–Galactic longitude–Galactic latitude (v, ℓ, b) , isosurface plot of $^{12}\text{CO}(1\text{-}0)$ emission at the $T_{\rm R}^*=4$ K level for the region of the Galactic Plane containing W51. The data are from the Massachusetts–Stony Brook Galactic Plane Survey (Sanders et al. 1986).
- Fig. 3.— Channel maps of the integrated $^{12}CO(J=1-0)$ emission in 2 km s⁻¹ intervals over the velocity range from 40-70 km s⁻¹. The values printed in the upper right corner of each panel denote the center of the velocity intervals. The grey scales in each panel are displayed in a logarithmic stretch from $\log_{10}(1.0 \text{ km s}^{-1})$ [white] to $\log_{10}(10.0 \text{ km s}^{-1})$ [black].
- Fig. 4.— Same as in Fig. 3, except for $^{13}CO(J=1-0)$. The grey scales in each panel are displayed in a logarithmic stretch from $\log_{10}(0.6 \text{ km s}^{-1})$ [white] to $\log_{10}(5.0 \text{ km s}^{-1})$ [black].
- Fig. 5.— *Top:* Histograms of the number of gaussians in the ¹²CO and ¹³CO data cubes as a function of the fitted mean velocity. *Bottom:* The total integrated intensity in the gaussian components as a function of the fitted mean velocity. The designated peaks denote a velocity component that occurs frequently in the ¹²CO and ¹³CO images, and the brackets show the range of velocities subjectively assigned to each component. The 58 km s⁻¹ velocity component is not a prominent feature as judged from this figure, but is included nonetheless since that is the velocity of the molecular gas associated with the brightest radio continuum emission.
- Fig. 6.— Various images of the W51 region. Left: Map of the $^{12}\text{CO}(1\text{--}0)$ integrated intensity $(\int T_{\rm R}^* dv)$ for gaussian fits with mean velocities between 56 to 71 km s⁻¹. The contour levels are 10, 25, 50, 100, and 200 K km s⁻¹. Center: Grey scale image of the 60μ m emission from the IRAS Sky Survey Atlas. The contours begin at $\log_{10}(100 \text{ MJy/ster})$ with logarithmic intervals of 0.15. Right: Map of the λ 21 cm radio continuum emission from Koo & Moon (1997). The contours levels are 0.015, 0.06, 0.12, 0.3, 1.0, and 2.4 Jy beam⁻¹. The dashed circle represents the 0.1 primary beam attenuation level, although the image itself has not been corrected for primary beam response. The prominent radio continuum sources are labeled in the λ 21 cm continuum image. The H II regions G49.4-0.3 and G49.5-0.4 are classically referred to as W51A, and G48.9-0.3, G49.1-0.4, and G49.2-0.4 as W51B. W51C has a nonthermal spectrum and is likely a supernova remnant.

Fig. 7.— Histogram of the 13 CO(1-0) integrated intensity for W51, the 68 km s⁻¹ cloud, and clouds associated with various H II regions that have been mapped in the similar manner (Carpenter, Snell, & Schloerb 1995; Heyer, Carpenter, & Ladd 1996). The histograms have been truncated at an intensity of 3 K km s⁻¹ since that is the highest 3σ detection limit among the various surveys. Assuming that the 13 CO emission is optically thin, the 13 CO abundance relative to H₂ is approximately constant, and the excitation conditions are similar, these histograms should reflect the relative H₂ column density distributions in these clouds.

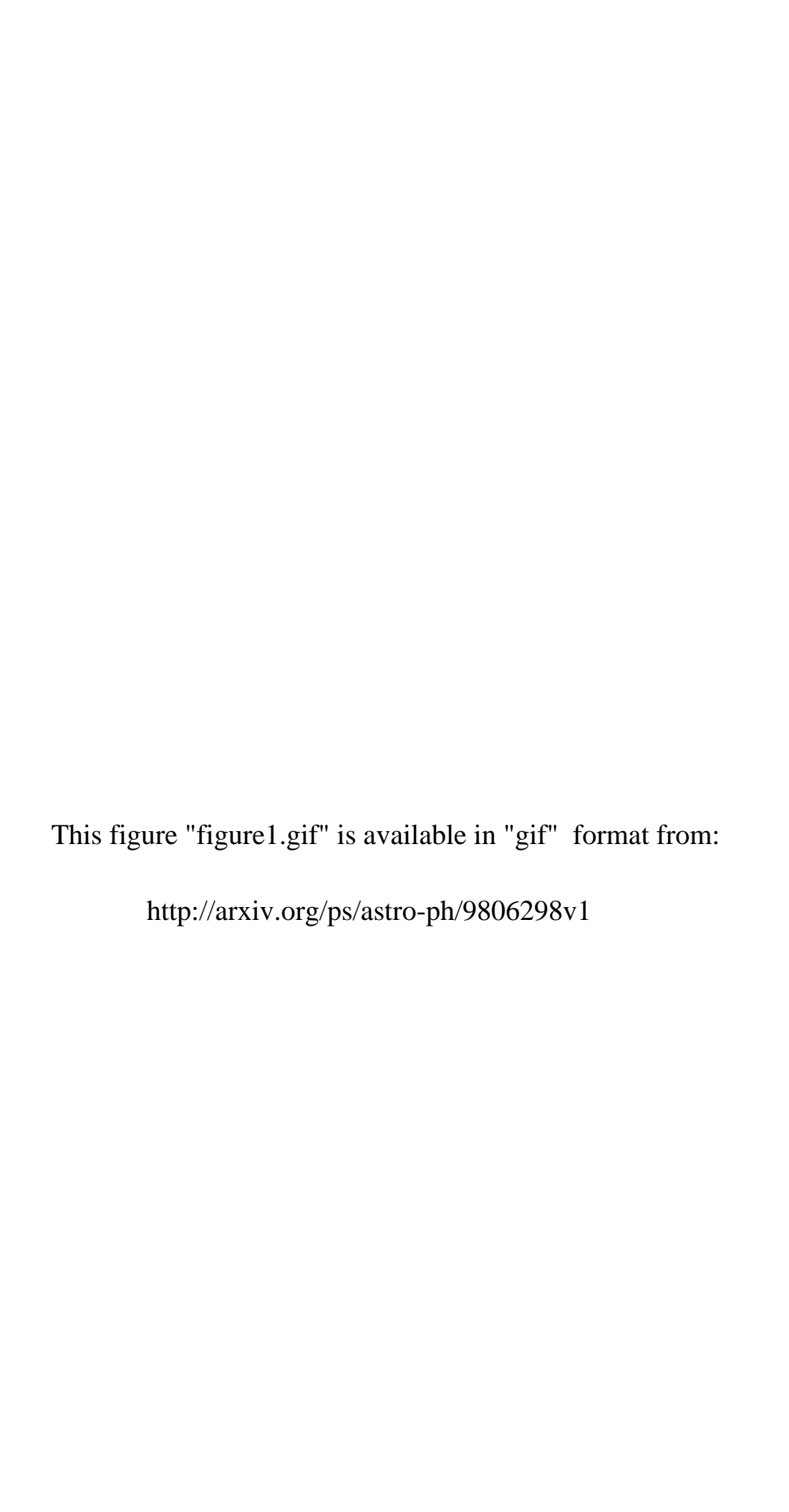


Table 1. Properties of the W51 and 68 $\rm km\,s^{-1}$ Clouds $^{\rm a}$

Cloud	$ heta_{ ext{min}} imes heta_{ ext{max}}$	$\Delta V_{ m FWHM}{}^{ m b}$	$M_{ m XCO}$	$M_{ m vir}$
	$(\mathrm{pc} \times \mathrm{pc})$	$({\rm km~s^{-1}})$	$(10^5 \mathrm{M_\odot})$	
W51	83 × 114	8.9	11.9	8.2
$68~{ m km~s^{-1}}$	22×136	4.6	1.9	

a — Assumed distance is 7.0 kpc (Genzel et al. 1981). b — Full width at half maximum of the sum of the $^{12}CO(1-0)$ gaussian fits

